Journal of Engineering Mechanics and Machinery (2026)
Clausius Scientific Press, Canada

DOI: 10.23977/jemm.2026.110214
ISSN 2371-9133 Vol. 11 Num. 2

Design of a Continuous Core-Removal Device for Loofah Sponge with Fiber-Rib Preservation

Jiayi Yang*, Lin Song, Yizhe Zhang, Minghai Xu, Jiaxing Wen, Xin Zhang

School of Mechanical and Electrical Engineering, Guilin University of Electronic Technology, Guilin, 541004, Guangxi, China
**Corresponding Author*

Keywords: Loofah sponge; Continuous core removal; Rib preservation; Finite element analysis; Modal analysis

Abstract: To address misalignment caused by blank rotation, damage to the fiber ribs, and poor structural integrity of finished products during continuous core removal, a continuous core-removal forming and rib-preservation device for loofah sponge was designed. The device consists of a frame, a feeding and conveying assembly, a slitting assembly, a spreading and exposing assembly, a core rough-cutting assembly, a flattening assembly, and a finish-planing core-removal unit. Using the blank's natural symmetrical cavities as positioning references, the blank is clamped and positioned so that the rotary slitting blade cuts a regular slit along the hollow cavities while avoiding the solid fiber ribs; the blank is then progressively spread by an inverted-triangular bracket followed by narrow and wide spreading members, and processed through multi-blade rough cutting, roller flattening and arc-blade finish planing, thereby establishing a three-stage sequential process for core removal, comprising "large-allowance rough cutting—flattening and shaping—profile finish planing". Key parameters such as the conveying speed, cutting force, cutter-shaft torque and motor power were theoretically calculated. Powered by 220 V single-phase electricity and driven independently by three motors, the device can adapt to loofah sponge blanks of different diameters and wall thicknesses, with a target core-removal rate of more than 95% while preserving the fiber ribs as much as possible.

1. Introduction

The object of this study is a loofah sponge blank whose outer skin has been removed while the inner core remains[1]. Its complete structure consists of the outer phloem, the middle-layer reticular fiber skeleton, and the inner-core tissue wrapping seeds, and these parts are cross-linked through fiber bundles and vascular tissues, forming a layered composite system with a dense exterior and a sparse interior and with markedly different hardness and toughness[2]. Loofah sponge is lightweight, porous, tough, and biodegradable. In addition to its traditional use as a cleaning material, it has been investigated as a functional material for oil–water separation[3]. Industrial surveys of loofah sponge in the producing areas represented by Xincheng County indicate that the related cultivation, processing and comprehensive utilization already have a regional industrial foundation[4].

Core removal, also referred to as pulp removal, is the key process by which a loofah sponge

blank is formed into a finished product with preserved fiber ribs, and its processing quality directly affects the grade of the finished product. Traditional processing mainly relies on manual beating, rolling, hollowing out, and cleaning, which are scattered operations, take a long time, and make product quality highly dependent on the operator's skill[5]. The few existing mechanized devices still need to further improve their adaptability to differences in the diameter, length, moisture content and posture of loofah sponge blanks so as to avoid fiber damage and inner-core residue during processing; the related mechanized schemes are found in the patent literature[6-8].

In terms of equipment research, existing Chinese studies have proposed methods involving mechanical cutting, rotary cutting, and auxiliary positioning[6-8]. These schemes provide references for the structural design of loofah sponge processing equipment, but there is still room for improvement in continuously adapting to the natural shape, internal cavities and fiber-rib distribution of loofah sponge blanks. Vision-based positioning and flexible grasping technologies have been applied in fruit and vegetable processing and robotic operations, and can provide references for the posture recognition and positioning of raw materials[9]. Overall, the existing equipment has not yet established a standardized continuous core-removal method for the natural shape and internal cavity structure of loofah sponge blanks, and problems such as misaligned processing and fiber-rib damage caused by blank rotation and individual differences still need to be solved.

To address the above problems, this paper designs a rib-preserving continuous core-removal device based on the internal structural feature of loofah sponge blanks, namely "multiple cavities with fiber ribs distributed between the cavities": through a dedicated positioning method, standardized clamping and positioning are realized so that cutting proceeds along the hollow cavities while avoiding the solid fiber ribs, and progressive spreading, rough cutting, flattening and finish planing are completed in sequence, so as to retain the fiber skeleton to the greatest extent while ensuring the core-removal rate and to provide equipment support for the large-scale and standardized processing of loofah sponge.

2. Overall Structure and Working Principle

2.1 Overall Structure

The overall structure of the rib-preservation processing device is shown in Figure 1. It mainly consists of seven parts: the frame, the feeding and conveying assembly, the slitting assembly, the spreading and exposing assembly, the core rough-cutting assembly, the flattening assembly, and the finish-planing core-removal unit. The frame is a horizontal framework welded from section steel, on which a cutting opening, a blade opening and a planing-blade opening are machined in sequence for the slitting blade, the rough-cutting blades and the finish-planing blade to pass through respectively. Along the conveying direction of the loofah sponge, the feeding and conveying assembly, the slitting assembly, the spreading and exposing assembly, the core rough-cutting assembly, the flattening assembly and the finish-planing core-removal unit are arranged in sequence. The machine is assembled in modules, has a compact structure, and is easy to disassemble, assemble, and maintain.

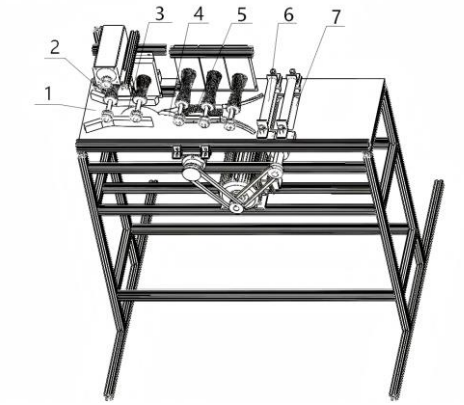


Figure 1: Three-Dimensional Structural Diagram of the Whole Device: 1—frame; 2—feeding and conveying assembly; 3—slitting assembly; 4—spreading and exposing assembly; 5—core rough-cutting assembly; 6—flattening assembly; 7—finish-planing core-removal unit

The main technical parameters of the device are shown in Table 1.

Table 1: Main Technical Parameters of the Device

Parameter	Value/Specification
Overall dimensions (length × width × height) / mm	1600 × 550 × 1100
Applicable loofah sponge blank diameter / mm	35–80
Applicable loofah sponge blank length / mm	150–400
Design conveying speed / (m/s)	0.05–0.15 (adjustable)
Design rough-cutting shaft speed / (r/min)	800–1500
Design finish-planing roller speed / (r/min)	1000–2000
Conveying motor (Motor 3) power / W	120
Slitting motor (Motor 2) power / W	120
Cutter motor (Motor 1) power / W	1500
Power supply	AC 220 V/50 Hz
Target core-removal rate / %	>95

2.2 Working Principle

The process flow of the device is shown in Figure 2. The processing object is preferably a semi-aged loofah sponge blank with an intact structure. During operation, the blank is first circumferentially positioned using its naturally symmetric internal cavities as positioning references, and the slitting depth is adjusted; then the feeding and conveying assembly clamps the blank and conveys it forward at a preset uniform speed. When the blank passes through the slitting assembly, the rotary slitting blade cuts a regular slit axially along the centerline of the cavity; afterwards, the tip of the inverted-triangular bracket first spreads the blank preliminarily, and then the narrow spreading member and the wide spreading member spread it gradually outward so that the inner core is fully exposed; the rotary blade set of the core rough-cutting assembly performs large-allowance rough cutting on the exposed inner core, removing more than 80% of the inner-core body; the metal roller of the flattening assembly squeezes the blank into a flat shape and eliminates wrinkles; finally, the arc-shaped conforming planing blade of the finish-planing core-removal unit performs profile finish planing along the flattened inner wall to completely remove the residual inner core. After cleaning and drying, the processed loofah sponge becomes a finished product with preserved fiber ribs.

The above process forms a three-stage sequential core-removal path of "large-allowance rough cutting—flattening and shaping—profile finish planing": rough cutting removes most of the inner core and reduces the load on the finish-planing unit, flattening ensures a flat surface for finish planing, and finish planing ultimately ensures complete core removal and controls the cutting depth so as not to damage the fiber ribs, thereby balancing core-removal efficiency and fiber integrity.

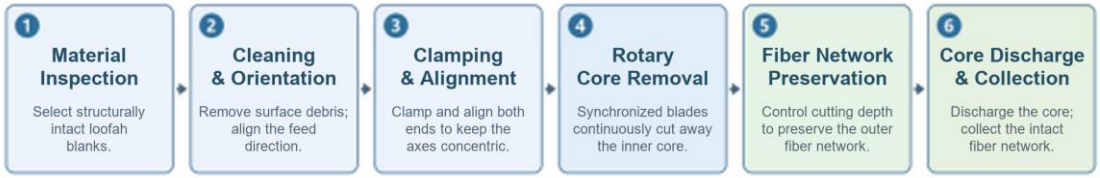


Figure 2: Block Diagram of the Processing Flow

3. Design of Key Components

3.1 Feeding and Conveying Assembly

The feeding and conveying assembly is responsible for clamping and conveying the loofah sponge blank at a uniform speed. Its structure is shown in Figure 3, and it consists of Motor 3, a driving sprocket, side plates, several conveying rollers, several driven sprockets, a first chain and several second chains. The ends of each conveying roller are hinged to the corresponding side plates. Motor 3 drives the driving sprocket, which drives one driven sprocket through the first chain; this driven sprocket then drives the remaining driven sprockets in sequence through the second chains, so that all the conveying rollers rotate in the same direction at the same speed and realize continuous, stable feeding of the loofah sponge blank. This two-stage chain transmission scheme ensures the speed consistency of the multiple rollers and works reliably in a fibrous dust environment; a similar guided conveying method has been verified in the feeding mechanisms of agricultural and forestry materials such as automatic bamboo cutting[10].

To balance the processing rhythm and the stability of the subsequent processes, the design conveying speed is v = 0.05–0.15 m/s, the design rated value is taken as v = 0.10 m/s, and the conveying-roller diameter is D = 50 mm; the rated speed of the conveying roller is then calculated by Eq. (1):

$$n = 60v/(\pi D) \tag{1}$$

Substituting the data gives n = 60×0.10/(π×0.05) ≈ 38.2 r/min; accordingly, the output speed of the geared motor is selected to be about 40 r/min. The surface of the conveying roller is diamond-knurled to increase the friction coefficient and prevent conveying slippage.

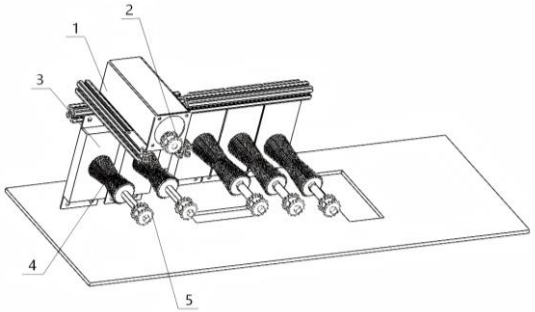


Figure 3: Structural Diagram of the Feeding and Conveying Assembly: 1—Motor 3; 2—driving sprocket; 3—side plate; 4—conveying roller; 5—driven sprocket

3.2 Slitting Assembly

The slitting assembly consists of a slitting blade and Motor 2. A cutting opening is machined on the frame; the slitting blade passes through this opening and is directly driven to rotate by Motor 2, actively slitting the loofah sponge blank while it is held in the prescribed position. Compared with passive slitting by a fixed blade, rotary slitting produces lower cutting resistance and a clean slit, and the cutting depth can be set uniformly by the adjusting structure on the side of the frame. The slit is cut axially along the centerline of the blank's cavity, with a depth that penetrates the outer phloem without cutting into the fiber ribs of the middle layer, thus providing a regular passage for the subsequent spreading assembly.

3.3 Spreading and Exposing Assembly

The spreading and exposing assembly adopts a fixed, unpowered inverted-triangular structure, consisting of an inverted-triangular bracket, a narrow spreading member and a wide spreading member, as shown in Figure 4. The inverted-triangular bracket is fixed to the frame; its tip first enters the loofah sponge blank, and then the narrow spreading member and the wide spreading member are connected in series. The widths of the three increase successively, so that the blank is progressively spread in a "preliminary spreading—transitional spreading—complete spreading" manner during conveying, until the inner core is fully exposed.

This assembly relies on the conveying motion of the blank itself to spread it passively along the wedge-shaped profile, requiring no independent power or active clamping mechanism. It is compatible with raw materials of different diameters and wall thicknesses without prior sorting and grading, and fundamentally avoids the forced pulling damage to fibers caused by active clamping. The progressive profile makes the spreading force increase gently, reducing the risk of fiber ribs being torn during spreading.

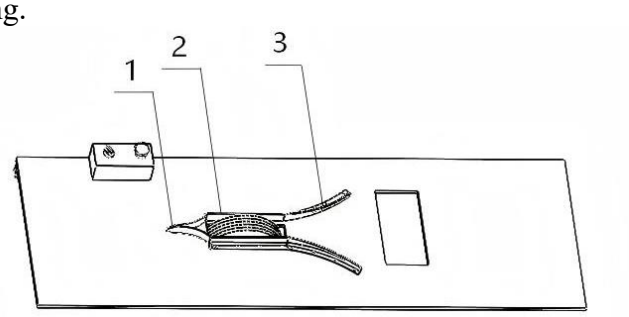


Figure 4: Structural Diagram of the Spreading and Exposing Assembly: 1—inverted-triangular bracket; 2—narrow spreading member; 3—wide spreading member

3.4 Core Rough-Cutting Assembly

The core rough-cutting assembly performs rough cutting with a large allowance and removes most of the inner core. It consists of a rotary blade set, a rotating shaft, drive belt 1, pulley 1 and a mounting bracket, as shown in Figure 5. The rotary blade set consists of 4–5 parallel disc blades, with adjacent blades spaced 2–5 mm apart and adjustable through spacers. The rotating shaft is supported on the frame through the mounting bracket, with the blade set mounted on one end and pulley 1 on the other end, and is driven to rotate by drive belt 1.

The inner core of the loofah sponge blank is a porous fiber material. Referring to the cutting characteristics of similar plant fibers, its shear strength is taken as τ = 0.3–0.8 MPa. The maximum cutting cross-sectional area of a single blade is estimated by $A = bh$; taking the cutting width b = 40

mm and the maximum cutting depth h = 3 mm, the maximum cutting force of a single blade is calculated by Eq. (2):

$$F_1 = \tau bh \tag{2}$$

Taking τ = 0.5 MPa gives F_1 = 0.5×40×3 = 60 N. Considering that no more than two blades participate in cutting simultaneously, the total cutting force is $F = 2F_1$ = 120 N. Taking the blade cutting radius r = 0.05 m, the torque required by the cutter shaft is calculated by Eq. (3):

$$T = Fr \tag{3}$$

Taking the design cutter-shaft speed n = 1200 r/min and the belt transmission efficiency η = 0.85, the power required by the cutter motor is calculated by Eq. (4):

$$P = 2\pi nT/(60\eta) \tag{4}$$

Substituting into Eq. (4) gives $P \approx$ 887 W. Considering the load fluctuation when Motor 1 simultaneously drives the finish-planing roller and cuts dry material, a 1500 W motor is selected in the design. The finite-element model assumes the severe design condition in which two blades participate in cutting simultaneously: design radial forces of 60 N in opposite directions are applied to the two blade mounting sections respectively, a design driving torque of +6 N·m is applied at the pulley input end, and a reverse cutting resistance torque of −3 N·m is applied to each of the two blade sections.

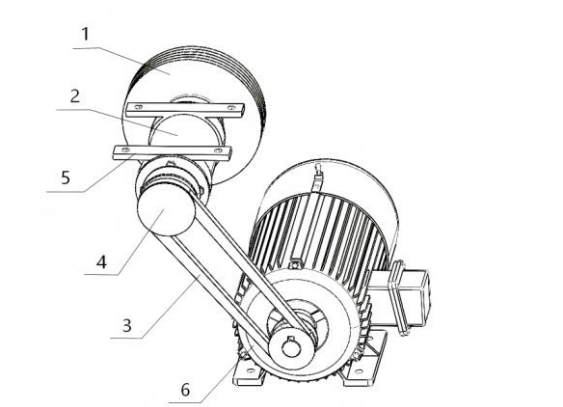


Figure 5: Structural Diagram of the Core Rough-Cutting Assembly: 1—rotary blade set; 2—rotating shaft; 3—drive belt 1; 4—pulley 1; 5—mounting bracket; 6—Motor 1

3.5 Flattening Assembly

The flattening assembly consists of a metal roller, an L-shaped plate, a screw and an L-shaped seat, as shown in Figure 6. The end of the metal roller is hinged to the L-shaped plate; the screw passes through the L-shaped plate and is connected to the L-shaped seat, which is fixed to the frame. The loofah sponge blank, after being spread and rough-cut, enters between the metal roller and the bottom plate of the frame; being pressed by the roller, it leaves the assembly in a flattened state, which eliminates the wrinkles produced by spreading and rough cutting so that it enters the finish-planing process with a flat surface. Rotating the screw changes the height of the L-shaped plate and thereby adjusts the gap between the metal roller and the bottom plate of the frame to adapt to raw materials with different wall thicknesses.

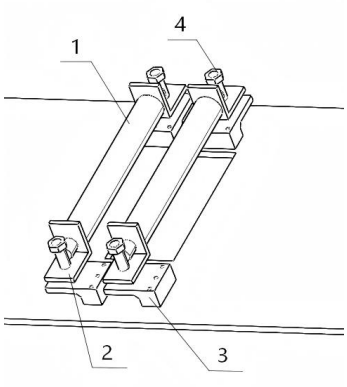


Figure 6: Structural Diagram of the Flattening Assembly: 1—metal roller; 2—L-shaped plate; 3—screw; 4—L-shaped seat

3.6 Finish-Planing Core-Removal Unit

The finish-planing core-removal unit is the final process that ensures the target core-removal rate. It consists of a position-limiting member, an arc-shaped conforming planing blade and its roller, pulley 2, drive belt 2, a driving pulley and Motor 1, as shown in Figure 7. Motor 1 drives the driving pulley, which drives pulley 2 through drive belt 2 and thereby drives the arc-shaped planing-blade roller to rotate. The position-limiting member is used to constrain the feeding position of the loofah sponge blank and ensure a stable planing depth. Referring to the general design experience of profile planing cutters for fruits and vegetables[11], the blade profile is designed according to the curvature of the inner wall of the flattened blank, and the design roller speed is taken as 1000–2000 r/min. The flattened blank passes through the planing zone at a constant speed, and the arc-shaped blade follows the inner-wall profile and scrapes off the thin residual inner-core layer and seeds left after rough cutting. Through the two-stage core removal of rough cutting and finish planing, the target core-removal rate is more than 95%, and the inner-core debris is collected centrally under the frame.

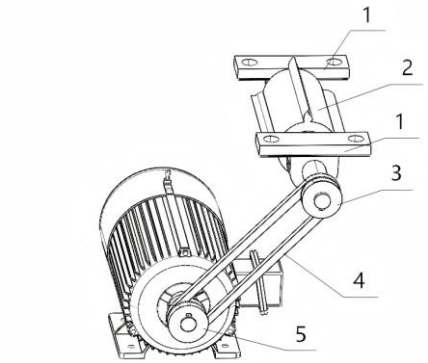


Figure 7: Structural Diagram of the Finish-Planing Core-Removal Unit: 1—position-limiting member; 2—arc-shaped conforming planing blade and roller; 3—pulley 2; 4—drive belt 2; 5—driving pulley

4. Transmission and Drive System Design

Three motors are used to independently drive three power trains: conveying, slitting, and cutting. The transmission layout is shown in Figure 8, and the speed of each process can be adjusted independently without mutual interference.

4.1 Conveying Chain Drive

The feeding and conveying assembly adopts a two-stage chain transmission: Motor 3 (a 120 W geared motor) drives the driving sprocket, transmits power to one driven sprocket through the first chain, and then drives all the conveying rollers in parallel through multiple second chains, ensuring strict synchronization of the multiple rollers and a constant feeding speed. Chain transmission has an accurate average transmission ratio and strong load-carrying capacity, and is suitable for dusty fiber environments, requiring only periodic grease lubrication in daily use.

4.2 Independent Slitting Drive

The slitting blade of the slitting assembly is directly driven by Motor 2 (120 W), so that its speed is independent of the conveying and cutter systems; the slitting speed can be adjusted separately according to the moisture content of the loofah sponge blank, and the cutting depth can be precisely controlled through the side adjusting mechanism of the frame.

4.3 Cutter Belt Drive

The core rough-cutting assembly and the finish-planing core-removal unit share Motor 1 (1500 W): the motor-side driving pulley engages with drive belts 1 and 2 simultaneously, which respectively drive the rough-cutting pulley 1 and the finish-planing pulley 2, so that one motor drives two rotary cutters in parallel and the transmission structure is simplified. The elasticity of the belt drive provides cushioning, absorbs instantaneous cutting impacts, and reduces vibration and noise; under overload, it slips to protect the cutter shaft and motor. By replacing pulleys of different diameters, the rough-cutting and finish-planing speeds can be adjusted separately to adapt to dry, hard blanks and wet, soft blanks.

4.4 Power Supply and Control

All three motors are powered by AC 220 V single-phase electricity, so there is no need to modify a three-phase industrial circuit, and the equipment can be used immediately upon installation. It can flexibly adapt to scenarios such as small-scale individual processing, cooperative mass production and factory-scale production. The electrical components of the whole machine are integrated into an independent control cabinet, whose panel is equipped with start, stop and emergency-stop buttons and a conveying-speed adjustment knob. The control logic is simple, and operators can operate the equipment after brief training.

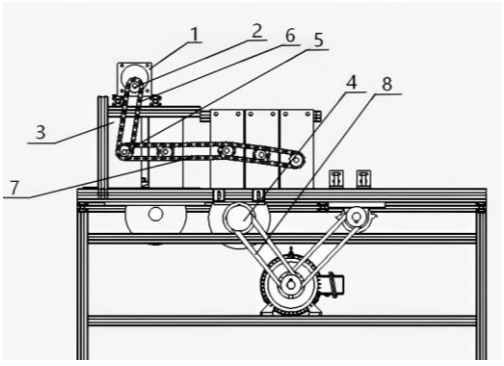


Figure 8: Structural Diagram of the Conveying Chain Transmission: 1—frame; 2—driving sprocket; 3—side plate; 4—pulley 1; 5—driven sprocket; 6—first chain; 7—second chain; 8—drive belt 1

5. Finite Element Analysis of Key Components

To verify the strength, stiffness and dynamic characteristics of the key load-bearing components under the design cutting conditions, this paper selects the body of the rough-cutting rotating shaft, which is subjected to the most severe load, as the object of finite element analysis. This object corresponds to the rotating shaft in the core rough-cutting assembly. The analysis is performed on the shaft body alone rather than on the entire machine or all attached parts as a single model. The analysis flow includes establishment of the finite element model, comparison of mesh accuracy and size, static analysis, zero-speed reference modal analysis, cutting-load prestressed modal analysis, and the 1200 r/min rotating prestressed modal recheck.

5.1 Establishment of the Finite Element Model

The three-dimensional model of the rough-cutting rotating shaft is established in SolidWorks, as shown in Figure 9. The file is a multi-body model, and 24 bodies are identified after importing into ANSYS Workbench. According to the component functions in Section 3.4 and the analysis objective of Section 5 of this paper, the main rotating-shaft body, which is continuous with the two-end supports and the blade mounting sections, is retained, while the blades, spacers and other attached bodies are suppressed. The original CAD file is not modified, and the suppression operation is applied only to the finite element analysis copy. Therefore, the object of the results in this paper is the "rough-cutting rotating shaft body", which is not equivalent to the complete cutter-shaft assembly containing all the blades and spacers. To control the computational scale, minor features such as keyways, chamfers and relief grooves that do not affect the overall load-bearing capacity are not separately refined. The shaft material is grade 45 steel, and its properties are taken according to the as-normalized condition (no specific heat treatment is specified): elastic modulus $E = 2.1\times10^5$ MPa, Poisson's ratio $\mu = 0.3$, density $\rho = 7.85\times10^3$ kg/m³, and yield strength $\sigma s = 355$ MPa. In the modal analysis, equivalent point masses of 1.225 kg each are applied to the two blade-mounting cylindrical surfaces; in the static analysis, these point masses are turned off.

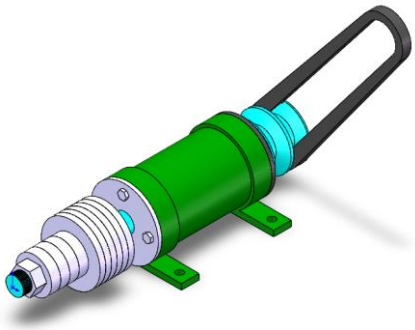


Figure 9: Three-Dimensional Model of the Rough-Cutting Shaft

5.2 Meshing and Boundary Conditions

ANSYS Workbench 2024 R2 is used for the analysis, with free meshing by second-order tetrahedral solid elements. Meshes with element sizes of 4, 3, and 2 mm were generated, and their size statistics are shown in Table 2. Comprehensively considering the ability to capture stress gradients near the blade mounting regions, shaft shoulders and supports, the computational accuracy and the solution scale, the 2 mm mesh is finally selected for the design load condition analysis. The 4 mm and 3 mm meshes are relatively coarse and are mainly used for comparing the model scale and computational cost; the 2 mm mesh can improve the local stress resolution at an acceptable

computational scale. Since the stress and deformation convergence data under the 4 mm and 3 mm meshes were not obtained, this paper describes this part as a "comparison of mesh accuracy and size" rather than as a complete mesh-independence verification. With the 2 mm mesh, the number of elements has reached 104 209, which is sufficient to capture the overall stress and deformation of the shaft. Therefore, further mesh refinement is unnecessary at this preliminary design stage. The shaft axis is taken along the global Z direction of the model. No tangential constraint is applied to the bearing support surfaces at the two ends, and only radial and axial supports are retained, so as to avoid balancing the transmitted torque with bearing reaction forces. A design torque of 6 N·m in the global +Z direction is applied to the power input end face of the pulley; design radial forces of 60 N in the global +Y and −Y directions are applied to the two blade mounting sections respectively, and a reverse cutting resistance torque of 3 N·m in the global −Z direction is applied to each; the gravitational acceleration of 9.80665 m/s² in the global −Y direction is also taken into account. The modal analysis takes into account the blade-spacer equivalent point mass of 1.225 kg at each of the two locations. The effective span between the two supports is about 160 mm.

Table 2: Comparison of Mesh Accuracy and Size of the Rough-Cutting Rotating Shaft and the Results under the 2 mm Design Condition

Mesh size/mm	Number of nodes	Number of solid elements	Maximum deformation/mm	Maximum equivalent stress/MPa	Maximum principal stress/MPa
4	66 937	38 166	—	—	—
3	104 266	58 965	—	—	—
2 (final)	183 449	104 209	0.009362	4.664	3.743

5.3 Static Analysis Results

The static results of the 2 mm final mesh under the modified design load are shown in Figures 10 and 11. The maximum total deformation is 0.009362 mm, the maximum equivalent stress is 4.664 MPa, and the maximum principal stress is 3.743 MPa. Using the 355 MPa yield strength of grade 45 steel, the maximum equivalent stress corresponds to a safety factor of about 76.1. Under the criterion of a two-support span $L \approx 160$ mm and a design allowable deformation $[w] = L/1000 = 0.160$ mm, the calculated deformation is about 5.85% of the design allowable value, indicating that the model provides sufficient stiffness margin. The 4 mm and 3 mm rows in Table 2 are retained only as references for mesh scale and computational cost; the static conclusions are based only on the 2 mm final mesh, and the results of different meshes are not mixed into the final conclusions.

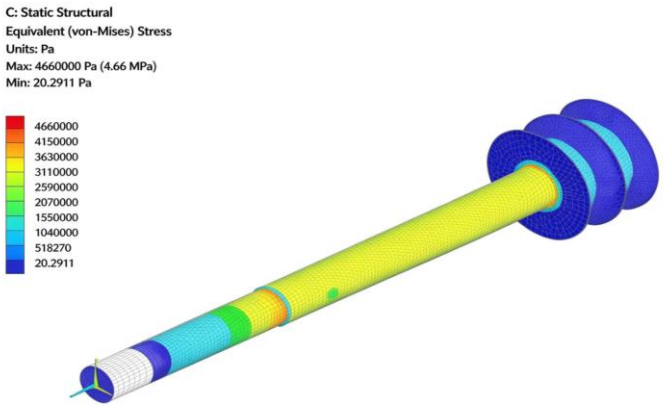


Figure 10: Equivalent Stress Contour of the Rough-Cutting Rotating Shaft under the Modified Design Load with the 2 mm Mesh

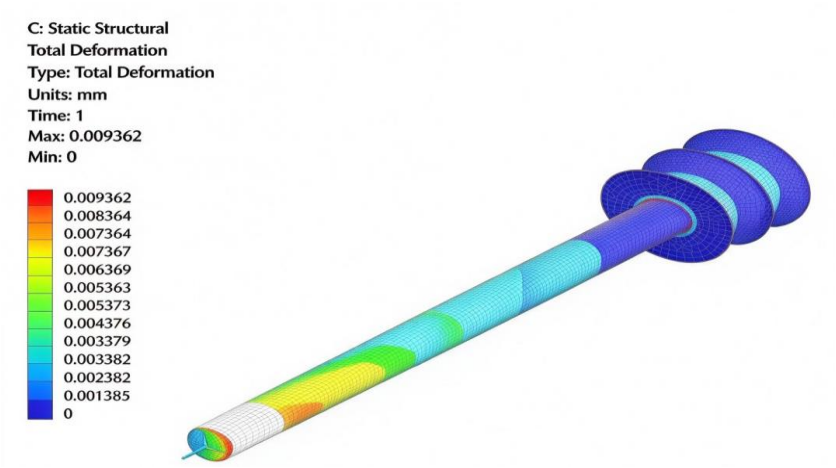


Figure 11: Total Deformation Contour of the Rough-Cutting Rotating Shaft under the Modified Design Load with the 2 mm Mesh

5.4 Modal Analysis

Under the same 2 mm mesh, material and support conditions, the zero-speed reference modal analysis, the cutting-load prestressed modal analysis and the 1200 r/min rotating prestressed modal analysis are carried out, with the blade-spacer equivalent point mass of 1.225 kg at each of the two locations taken into account, and the first six natural frequencies and mode shapes are extracted; the results are shown in Table 3, Figure 12 and Figure 13. The first six natural frequencies under the zero-speed reference condition are 316.621, 319.147, 350.709, 1463.904, 2054.315 and 2155.899 Hz; the first six natural frequencies under the cutting-load prestressed condition are 316.625, 319.145, 350.724, 1463.904, 2054.315 and 2155.903 Hz; and the first six natural frequencies under the 1200 r/min rotating prestressed condition are 316.055, 318.567, 350.723, 1463.903, 2054.315 and 2155.847 Hz. The design speed of the cutter shaft is 1200 r/min, corresponding to a design operating frequency of 20 Hz. Taking 20 Hz as the reference, the ratios of the first six natural frequencies of the rotating prestressed condition to the design operating frequency are 15.80, 15.93, 17.54, 73.20, 102.72 and 107.79 respectively; the first-order frequency corresponds to the minimum frequency margin and is the controlling order, so Figures 12 and 13 mainly present the first-order mode shape, while the other orders are listed and compared in Table 3. For rotating-shaft parts, the low-order bending modes are the ones most easily excited by the operating speed. In this model, the natural frequencies from the fourth mode onward are all higher than 1400 Hz, reaching more than 70 times the operating frequency, so no resonance is expected under the analyzed conditions; therefore only the first-order controlling mode shape is presented, and the frequencies of the other orders are listed in Table 3. The modal contours are displayed with normalized mode shapes, and the graphical amplitudes do not represent the actual operating displacement of the shaft, so the bending amplitudes of different conditions should not be directly compared. The first-order frequencies of the zero-speed and 1200 r/min rotating prestressed conditions differ by only about 0.179%, indicating that the rotation effect has little influence on the overall mode shape of this model. The above frequencies were obtained from a batch reanalysis in ANSYS MAPDL and are not measured values of a prototype.

Table 3: First Six Natural Frequencies of the Rough-Cutting Rotating Shaft (2 mm mesh, with equivalent point mass; the third column is the cutting-load prestressed/1200 r/min rotating prestressed)

Order	Zero-speed reference/Hz	Prestressed/Rotating prestressed/Hz
1	316.621	316.625 / 316.055
2	319.147	319.145 / 318.567
3	350.709	350.724 / 350.723
4	1 463.904	1 463.904 / 1 463.903
5	2 054.315	2 054.315 / 2 054.315
6	2 155.899	2 155.903 / 2 155.847

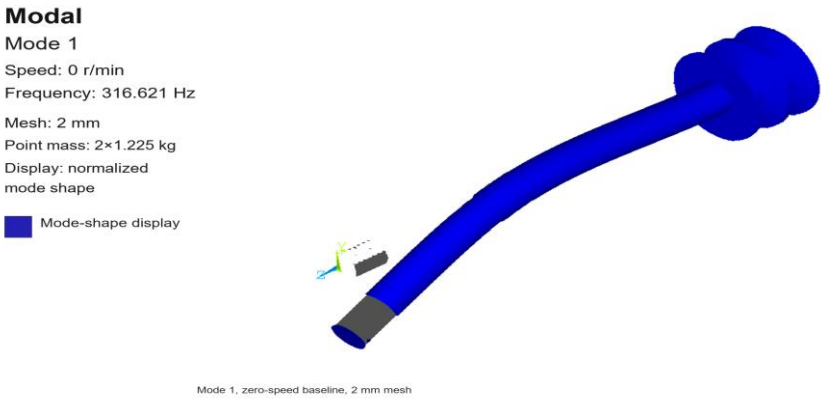


Figure 12: First-Order Mode Shape of the Rough-Cutting Rotating Shaft (2 mm mesh, zero-speed reference)

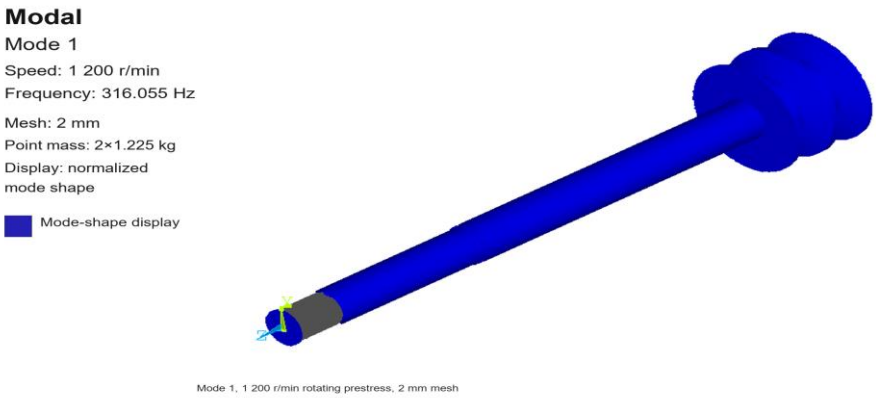


Figure 13: First-Order Mode Shape of the Rough-Cutting Rotating Shaft (2 mm mesh, 1200 r/min rotating prestressed)

5.5 Limitations of the Simulation

The model suppresses minor structures such as keyways and chamfers, so the obtained stress mainly reflects the overall response of the smooth shaft body, and the local stress concentration at the keyways is not evaluated. The bearings adopt idealized supports, and the flexibility of the actual bearings is not taken into account. The static condition does not take into account the rotating centrifugal load; the separate 1200 r/min rotating prestressed modal analysis takes into account the rotation effect but not more complex rotor-dynamic factors such as gyroscopic damping.

6. Conclusion

To solve the problems of rotation-induced misalignment of raw materials, damage to the fiber ribs, and poor structural integrity of finished products during the continuous core removal of loofah sponge, this paper designs a rib-preserving continuous core-removal device based on the multi-cavity internal structural feature of loofah sponge blanks, and draws the following conclusions:

(1) The device consists of seven functional components, namely the frame, feeding and conveying, slitting, spreading and exposing, core rough-cutting, flattening and finish-planing core-removal components, thereby establishing a three-stage sequential process for core removal, comprising "large-allowance rough cutting—flattening and shaping—profile finish planing", which is used for the continuous core-removal forming of loofah sponge blanks.

(2) The device adopts a circumferential positioning method based on the natural symmetrical cavities of the blank, which both restricts the rotation of the raw material and makes the slitting line run along the hollow cavities while avoiding the solid fiber ribs, and can support standardized rib-preserving cutting.

(3) A scheme combining unpowered progressive spreading, multi-blade rough cutting and arc-shaped profile finish planing is adopted, and key parameters such as the design conveying-roller speed, design cutting force, design cutter-shaft torque and design motor power are determined through theoretical calculation. With three independently driven motors and 220 V single-phase power supply, the device has a simple structure and convenient maintenance, can adapt to multi-specification raw materials with diameters of 35–80 mm, and has a target core-removal rate of more than 95%.

(4) The body of the rough-cutting rotating shaft is verified by finite element analysis. Under the modified design load and the 2 mm mesh, the maximum equivalent stress is 4.664 MPa, far lower than the 355 MPa yield strength of grade 45 steel, indicating a large design strength margin; the maximum total deformation is 0.009362 mm, accounting for only 5.85% of the design allowable deformation of 0.160 mm. After the equivalent masses of the blades and spacers are taken into account, the first-order frequencies of the zero-speed, cutting-load prestressed and 1200 r/min rotating prestressed conditions are 316.621, 316.625 and 316.055 Hz respectively, and the first natural frequency under the rotating prestressed condition is approximately 15.8 times the design operating frequency of 20 Hz. The ratios of the first six frequencies to the operating frequency are all not lower than 15.80, and the first order is the controlling order with the minimum frequency margin, so the mode-shape figures mainly present the first order. The above conclusions are limited to the current linear model, equivalent point mass and idealized support assumptions.

Acknowledgement

This work was supported by the Autonomous Region-Level College Students' Innovation and Entrepreneurship Training Program (S202610595321).

References

[1] Chinese Pharmacopoeia Commission. Pharmacopoeia of the People's Republic of China: 2020 Edition, Volume I [S]. Beijing: China Medical Science Press, 2020.

[2] Ai Xiaolin, Chen Yandan, Huang Biao, et al. Research progress on comprehensive utilization of loofah sponge fiber [J]. Chemical Industry and Engineering Progress, 2015, 34(6): 1708-1713, 1729.

[3] Yan Hongqin, Zheng Wenrui, Zhang Guiyu, et al. Preparation of hydrophobic/oleophilic loofah sponge and its application in oil–water separation [J]. Chemical Industry and Engineering Progress, 2021, 40(5): 2893-2899.

[4] Lin Shengyue, Liang Wenying, Mo Ningzheng, et al. Investigation and research on the development of loofah sponge industry in Xincheng County [J]. Jiangxi Agriculture, 2024(15): 145-148.

[5] Zhong Chuan. Harvesting and processing method of loofah sponge [J]. Practical Rural Technology, 2001(3): 58.
[6] Lai Xiaotao. A device for progressive fixed-length cutting of loofah sponge: CN202110376401.7 [P]. 2021-07-16.
[7] Guo Qingdao. Loofah sponge sawing device: CN202322568144.4 [P]. 2023-09-21.
[8] Geng Lina, Chen Lusheng. A machine for peeling, cutting and removing seeds of loofah to make loofah sponge: CN109129616A [P]. 2019-01-04.
[9] XU H T. Vision-based mobile robotic arm object gripping and handling [C]//AIP Conference Proceedings: Vol.3144. [S.l.]: AIP Publishing, 2024: 030012.
[10] Kang Kai, Zhou Yao, Liu Xinjie, et al. Design of an automatic bamboo cutting machine [J]. Southern Agricultural Machinery, 2025, 56(19): 135-137.
[11] Jin Hongchao. An improved fruit and vegetable peeler: CN201220754537.0 [P]. 2013-06-19.